Finite Element Simulation of Compressible Particle-Laden Gas Flows

Marcel Gurris, Dmitri Kuzmin and Stefan Turek

Institute of Applied Mathematics (LS III), Dortmund University of Technology
Vogelpothsweg 87, 44227 Dortmund, Germany

Abstract

A macroscopic two-fluid model of compressible particle-laden gas flows is considered. The governing equations are discretized by a high-resolution finite element method based on algebraic flux correction. A multidimensional limiter of TVD type is employed to constrain the local characteristic variables for the continuous gas phase and conservative fluxes for a suspension of solid particles. Special emphasis is laid on the efficient computation of steady state solutions at arbitrary Mach numbers. To avoid stability restrictions and convergence problems, the characteristic boundary conditions are imposed weakly and treated in a fully implicit manner. A two-way coupling via the interphase drag force is implemented using operator splitting. The Douglas-Rachford scheme is found to provide a robust treatment of the interphase exchange terms within the framework of a fractional-step solution strategy. Two-dimensional simulation results are presented for a moving shock wave and for a steady nozzle flow.

Key words: Particle-laden gas flows, inviscid two-fluid model, Euler equations, unstructured meshes, implicit high-resolution schemes

1. Introduction

Compressible flows of an inviscid gas carrying small particles or droplets commonly occur in nature and in industrial equipment. Their applications in science and engineering include dusty detonations, condensation in a (nuclear) power plant, volcanic eruptions, diesel injection into an engine, and spraying processes. In recent years, computational fluid dynamics (CFD) has gained popularity as a tool for investigation of such problems.

During the past few decades, many mathematical models and numerical methods have been developed for multiphase/multicomponent flows. Most numerical studies are concerned with incompressible gas-liquid mixtures. At the macroscopic level, a two-fluid model is set up using postulation or averaging theory [5]. The result is a system of balance laws that can be solved, for example, by a pressure correction scheme like SIMPLE (Semi-Implicit Method for Pressure-Linked Equations) with strong coupling via the interphase slip/partial elimination algorithm (IPSA/PEA).

In contrast to significant recent advances in the development of CFD methods for disperse gas-liquid flows, publications dealing with macroscopic two-fluid models of compressible particle-laden gas flows have remained relatively scarce. In most cases, computations are performed by (explicit) finite volume schemes [14, 15, 16, 17] in 1D or using dimensional splitting. A notable exception to this rule is the adaptive finite element flux-corrected transport (FEM-FCT) algorithm developed by Sivier *et al.* [12, 18] for simulation of dusty shock flows on unstructured meshes.

The numerical treatment of boundary conditions for compressible two-phase flows is rarely discussed in the literature, although it requires special care even in the case of a pure gas [2, 7, 19]. Moreover, the widespread use of explicit schemes is not to be recommended for steady-state computations, especially in the presence of low Mach number regions. Implicit methods are better suited for marching the solution to a steady state but their implementation in a multiphase CFD code must ensure a proper interplay of all algorithmic components (discretization, linearization, boundary conditions, preconditioning etc.) to achieve high performance.

The research reported in the present paper is aimed at the development of a strongly implicit high-resolution finite element scheme for an inviscid two-phase flow model. A challenging long-term goal is numerical simulation of arc spraying processes. In a typical industrial application, a carrier gas is injected into a nozzle at high pressure. Small metallic particles are created by melting an arc wire and shot onto a substrate, where solidification takes place. This simple technology results in a very robust coating.

The remainder of this paper is organized as follows. The employed mathematical model is presented in the next section. Next, the discretization and iterative solution of the governing equations are addressed. The topics to be covered include algebraic flux correction, numerical treatment of nonlinearities, implementation of boundary conditions, and operator splitting. Finally, simulation results are presented for 2D test problems.

2. Mathematical Model

Eulerian models of particle-laden gas flows are based on macroscopic conservation laws that can be derived by averaging the (exact) single-phase balance equations. The averaging procedure presented by Drew and Passman [5] yields a set of partial differential equations that express the conservation of mass, momentum, and energy for the continuous gas phase (index g) and dispersed particles (index p). The inviscid two-fluid model reads

$$\begin{aligned}
\partial_t(\alpha_g\rho_g) + \nabla\cdot(\alpha_g\rho_g\mathbf{u}_g) &= 0, && (1)\\
\partial_t(\alpha_g\rho_g\mathbf{u}_g) + \nabla\cdot(\alpha_g(\rho_g\mathbf{u}_g\otimes\mathbf{u}_g + P_g\mathcal{I})) &= P_g^i\nabla\alpha_g - \mathbf{f}_D, && (2)\\
\partial_t(\alpha_g\rho_g E_g) + \nabla\cdot(\alpha_g(\rho_g E_g + P_g)\mathbf{u}_g) &= \mathbf{u}^i\cdot(P_g^i\nabla\alpha_g - \mathbf{f}_D) - q_T, && (3)\\
\partial_t(\alpha_p\rho_p) + \nabla\cdot(\alpha_p\rho_p\mathbf{u}_p) &= 0, && (4)\\
\partial_t(\alpha_p\rho_p\mathbf{u}_p) + \nabla\cdot(\alpha_p(\rho_p\mathbf{u}_p\otimes\mathbf{u}_p + P_p\mathcal{I})) &= P_p^i\nabla\alpha_p + \mathbf{f}_D, && (5)\\
\partial_t(\alpha_p\rho_p E_p) + \nabla\cdot(\alpha_p(\rho_p E_p + P_p)\mathbf{u}_p) &= \mathbf{u}^i\cdot(P_p^i\nabla\alpha_p + \mathbf{f}_D) + q_T, && (6)
\end{aligned}$$

where α_k, ρ_k, u_k, P_k and E_k are the volume fraction, density, velocity, pressure, and specific total energy of phase k. The interfacial pressures and velocity are denoted by P_k^i and $\mathbf{u}^i$, respectively. The rate of interphase momentum and energy transfer due to the viscous drag force and heat exchange is given by the source/sink terms $\mathbf{f}_D$ and q_T to be defined below. No other interphase transfer mechanisms are considered in this work.

We suppose that the flow is dilute and P_g satisfies the ideal gas law. The particles are rigid, so the interfacial pressures are assumed to be zero, i.e., $P_p^i = P_g^i = 0$. Due to the small volume fraction of particles in dilute flows, particle collisions are neglected, and we consider the particulate phase to be pressureless, i.e., $P_p = 0$. Furthermore, $\mathbf{u}^i$ is approximated by $\mathbf{u}_p$. With these simplifications and $P := P_g$, our model (1)–(6) can be written as

$$\begin{aligned}
\partial_t(\alpha_g\rho_g) + \nabla\cdot(\alpha_g\rho_g\mathbf{u}_g) &= 0, && (7)\\
\partial_t(\alpha_g\rho_g\mathbf{u}_g) + \nabla\cdot(\alpha_g(\rho_g\mathbf{u}_g\otimes\mathbf{u}_g + P\mathcal{I})) &= -\mathbf{f}_D, && (8)\\
\partial_t(\alpha_g\rho_g E_g) + \nabla\cdot(\alpha_g(\rho_g E_g + P)\mathbf{u}_g) &= -\mathbf{u}_p\cdot\mathbf{f}_D - q_T, && (9)\\
\partial_t(\alpha_p\rho_p) + \nabla\cdot(\alpha_p\rho_p\mathbf{u}_p) &= 0, && (10)\\
\partial_t(\alpha_p\rho_p\mathbf{u}_p) + \nabla\cdot(\alpha_p\rho_p\mathbf{u}_p\otimes\mathbf{u}_p) &= \mathbf{f}_D, && (11)\\
\partial_t(\alpha_p\rho_p E_p) + \nabla\cdot(\alpha_p\rho_p E_p\mathbf{u}_p) &= \mathbf{u}_p\cdot\mathbf{f}_D + q_T. && (12)
\end{aligned}$$

The particle mass density ρ_p is assumed to be constant in these equations.

Since the continuous and disperse phase must fill the whole space, their volume fractions are coupled by the saturation constraint

$$\alpha_g + \alpha_p \equiv 1. \tag{13}$$

The lack of pressure in the particulate phase equations may give rise to delta shocks, and the effective particle density may become unbounded. In the case of the two-fluid model, these nonphysical phenomena are not observed [15], which can be attributed to the work of the drag force and heat exchange. The assumption of dilute flow is essential. Otherwise, particle collisions are nonnegligible and should be taken into account.

To close the system, a few constitutive laws need to be specified. The total energies E_k are expressed in terms of the internal energies ϵ_k

$$E_g = \epsilon_g + \frac{1}{2}|\mathbf{u}_g|^2, \qquad E_p = \epsilon_p + \frac{1}{2}|\mathbf{u}_p|^2. \tag{14}$$

The internal energies are proportional to the temperatures denoted by T_k

$$\epsilon_g = c_{vg} T_g, \qquad \epsilon_p = c_{vp} T_p, \tag{15}$$

where c_{vg} are c_{vp} are the specific heats at constant volume. The pressure, density, and energy of an ideal gas are related by the equation of state

$$P = (\gamma - 1)\rho_g \epsilon_g \tag{16}$$

in which γ is the constant ratio of specific heats. Since the density of particles ρ_p exceeds the gas density ρ_g by orders of magnitude, the virtual mass force is neglected. The lift force, gravity, and other interfacial effects are also negligible [12] as compared to the viscous drag force defined as

$$\mathbf{f}_D = \frac{3}{4} C_D \frac{\alpha_p \rho_g}{d} |\mathbf{u}_g - \mathbf{u}_p|(\mathbf{u}_g - \mathbf{u}_p). \tag{17}$$

In this formula, d is the particle diameter, and C_D is a dimensionless drag coefficient which is assumed to be a function of the Reynolds number

$$Re = \frac{\rho_g d |\mathbf{u}_g - \mathbf{u}_p|}{\mu_g}. \tag{18}$$

The dependence of C_D on Re is given by the widely accepted correlation

$$C_D = \begin{cases} \frac{24}{Re}(1 + 0.15Re^{0.687}), & \text{if} \quad Re < 1000, \\ 0.44, & \text{if} \quad Re \geq 1000. \end{cases} \tag{19}$$

The rate of heat transfer is proportional to the temperature difference

$$q_T = \frac{Nu 6\kappa_g}{d^2}\alpha_p(T_g - T_p), \tag{20}$$

where the Nusselt number Nu is a function of the Prandtl number Pr

$$Nu = 2 + 0.65Re^{\frac{1}{2}}Pr^{\frac{1}{3}}, \qquad Pr = \frac{c_{pg}\mu_g}{\kappa_g}. \tag{21}$$

The thermal conductivity κ_g, heat capacity at constant pressure c_{pg}, and (microscopic) dynamic viscosity μ_g of gas are assumed to be constant.

3. Numerical Method

The equations of the two-fluid model are discretized using (bi-)linear finite elements on an unstructured mesh. Algebraic flux correction of TVD type [10, 11] is performed to suppress spurious oscillations. All the necessary information is inferred from the discrete operators, which makes this approach very flexible and applicable in arbitrary dimensions. Therefore, an extension of the current 2D implementation to 3D is straightforward.

In this work, we are mainly interested in steady state solutions. Since explicit schemes are subject to severe stability restrictions, we discretize in time using implicit methods. In particular, the unconditional (linear) stability of the backward Euler scheme makes it a good choice for steady state computations. An implicit approach is also suitable for nonstationary problems, especially if a nonuniform distribution of Courant numbers renders the stability constraints for explicit algorithms too restrictive.

3.1. Coupled System

The PDE system (7)–(12) can be written in the compact generic form

$$\partial_t U + \nabla \cdot F(U) = S(U), \tag{22}$$

where U is the vector of conservative variables, F is the flux tensor, and S is the vector of source terms that introduce a two-way coupling and give

rise to an additional nonlinearity in the model. In the case of small particles, the dominance and stiffness of S slow down convergence of implicit schemes and aggravate stability restrictions in explicit computations. To circumvent this problem, we take advantage of operator splitting.

3.1.1. Yanenko Splitting

A popular approach to solving (22) is the Yanenko splitting (cf. [15, 17])

$$\frac{U^* - U^n}{\Delta t} + \nabla \cdot F^* = 0, \tag{23}$$

$$\frac{U^{n+1} - U^*}{\Delta t} = S^{n+1}. \tag{24}$$

In the first step, the numerical solution is advanced in time without taking the source terms into account. In the second step, the nodal values of the resulting solution U^* are corrected by adding the contribution of S^{n+1}.

For an explicit solver, the Yanenko splitting is a good choice, although it is only first-order accurate. However, the complete decoupling of the source term has an adverse effect on the performance of implicit schemes in steady-state computations. Due to the lagged application of S^{n+1}, the end-of-step solution U^{n+1} does not satisfy the equations of the first subproblem. Hence, the number of iterations does not decrease in the steady state limit, and an important advantage of the implicit approach is lost.

3.1.2. Douglas-Rachford Splitting

To make sure that the splitting does not disturb solutions approaching a steady state, we replace (23)–(24) by the Douglas-Rachford scheme [4]

$$\frac{U^* - U^n}{\Delta t} + \nabla \cdot F^* = S^n, \tag{25}$$

$$\frac{U^{n+1} - U^*}{\Delta t} = S^{n+1} - S^n \tag{26}$$

which is known to be very robust, at least in the context of alternating direction implicit (ADI) iterative solvers for multidimensional problems.

Obviously, the implicit correction in the second step does not change a converged stationary solution. Moreover, the Douglas-Rachford splitting provides a closer link between the density and velocity of the particulate phase. This is another reason why it is preferred to the Yanenko splitting.

3.2. Finite Element Solvers

Let us begin with the transport step (25) in which the source terms are treated explicitly and reside in the right-hand side. Without these terms, the system of conservation laws for the gas phase (7)–(9) exhibits the same structure as the compressible Euler equations. The equations of the particulate phase (10)–(12) describe the convective transport of mass, momentum, and energy by the velocity field $\mathbf{u}_p$. Although the two systems are coupled via the saturation constraint (13), they can be solved sequentially using numerical methods for semi-discrete problems of the form (25).

3.2.1. Galerkin Discretization

Multiplying system (25) by a test function, integrating over the domain, and using a set of piecewise-polynomial basis functions $\{\varphi_j\}$ to approximate U and F, one obtains the Galerkin finite element discretization

$$\sum_j \int_\Omega \varphi_i \varphi_j d\mathbf{x} \left[\frac{U_j^* - U_j^n}{\Delta t} - S_j^n \right] + \sum_j \int_\Omega \varphi_i \nabla \varphi_j d\mathbf{x} \cdot F_j^* = 0. \tag{27}$$

Using integration by parts, the second term can be represented in the form

$$\sum_j \int_\Omega \varphi_i \nabla \varphi_j d\mathbf{x} \cdot F_j^* = \sum_j \int_{\partial\Omega} \varphi_i \varphi_j \mathbf{n} ds \cdot F_j^* - \sum_j \int_\Omega \varphi_j \nabla \varphi_i d\mathbf{x} \cdot F_j^*, \tag{28}$$

where $\mathbf{n}$ is the unit outward normal to the boundary $\partial\Omega$. This form is amenable to implementation of weak boundary conditions (see below).

Invoking the homogeneity property of inviscid fluxes, we end up with a nonlinear algebraic system for the vector of discrete nodal values

$$\left[MU^* - \Delta t K(U^*) \right] U^* = MU^n + \Delta t G^n. \tag{29}$$

Here M denotes the (lumped) mass matrix and K is the discrete transport operator. The load vector G^n combines the contribution of the discretized source term S^n and weakly imposed boundary conditions, if any.

3.2.2. Algebraic Flux Correction

The left-hand side matrix for the standard Galerkin discretization (29) of a hyperbolic system is known to possess very unfavorable properties. As a consequence, solutions are frequently corrupted by spurious oscillations, and iterative solvers may fail to converge. Within the framework of

algebraic flux correction [10], such troubles are ruled out using an adaptive mechanism to control the 'bad' part of the matrix K. To this end, a nonoscillatory low-order counterpart of (29) is constructed by adding artificial viscosity. The difference between the residuals of the high- and low-order schemes is decomposed into internodal fluxes that are tuned to minimize the loss of accuracy. In this work, the admissible magnitude of each flux is determined by a multidimensional limiter of TVD type [11].

Gas Phase Equations. Algebraic flux correction for the hyperbolic system of gas phase equations is performed in terms of local characteristic variables, as explained in [10, 11] in the context of the compressible Euler equations.

Particle Equations. Since there is no pressure in the particle equations, all information is transported by a single wave traveling with velocity $\mathbf{u}_p$. The discrete transport operator K is block-diagonal, and algebraic flux correction is carried out using scalar limited dissipation proportional to

$$d_{ij} = \max\{|k_{ij}|, |k_{ji}|\} = d_{ji}, \qquad \forall j \neq i. \tag{30}$$

This definition of the artificial diffusion coefficient d_{ij} leads to a scalar version of the Rusanov scheme which produces physically correct solutions. Flux limiting is performed in terms of the conservative variables. In contrast to the gas phase equations, a transformation to characteristic variables is neither possible nor necessary. Despite the use of scalar dissipation, the nonlinear algebraic system is solved in a fully coupled manner.

3.2.3. Boundary Conditions

Boundary conditions play an important role in the design of numerical methods for inviscid compressible flows. If insufficient care is taken in the imposition and numerical implementation of boundary conditions, this may inhibit or significantly degrade convergence of the nonlinear iteration. An explicit or semi-implicit boundary treatment may also restrain the range of admissible time steps, rendering an otherwise implicit solution strategy inefficient [20]. Hence, a genuinely implicit implementation is a prerequisite for the development of a robust and fast nonlinear solver.

Following Selmin and Formaggia [19], we prescribe boundary conditions in a weak sense. That is, a boundary flux is defined using the input data and/or the solution of a Riemann problem [20]. Fluxes evaluated at the quadrature points are used to assemble the surface integral that arises

in (28) after integration by parts. The associated volume integral remains unchanged. At solid walls, we currently enforce the no-penetration condition by projecting the residual of the nonlinear algebraic system onto the tangent at each outer iteration. This strategy provides an equal treatment of both phases and does not produce spurious layers which are observed otherwise.

Gas Phase Equations. The solution of the gas phase Euler equations is a superposition of waves moving in different directions. Therefore, boundary conditions are to be prescribed in terms of the Riemann invariants [7]

$$W_1 = v_n - \frac{2c}{\gamma - 1}, \quad W_2 = \frac{P}{\rho^\gamma}, \quad W_3 = v_t, \quad W_4 = v_n + \frac{2c}{\gamma - 1}. \tag{31}$$

Here c is the local speed of sound, while v_n and v_t are the normal and tangential velocity, respectively. The associated characteristic speeds are

$$\lambda_1 = v_n - c, \quad \lambda_2 = v_n, \quad \lambda_3 = v_n, \quad \lambda_4 = v_n + c. \tag{32}$$

The incoming and outgoing waves are treated differently. To evaluate the flux at a given quadrature point, the vector of numerical boundary values is transformed to the Riemann invariants (31). The ones associated with nonnegative eigenvalues λ_k are left unchanged, while the rest is overwritten by the physical boundary conditions [10]. The result is transformed back to the conservative variables. Finally, the boundary flux is evaluated using an approximate or exact Riemann solver, as applied to the original and modified solution vectors. For details, the interested reader is referred to [6, 9, 20]. It is worth mentioning that it is possible to prescribe the Riemann invariants in such a way that the primitive variables are fixed [7].

Particle Equations. In the pressureless particulate phase, all flow variables are transported by a single wave. Therefore, weakly imposed boundary conditions can be implemented as in the case of scalar conservation laws, and there is no need for variable transformations. At the inlets ($\mathbf{n} \cdot \mathbf{u}_p < 0$), the fluxes are evaluated using the prescribed boundary values, while the current values of the numerical solution are employed to compute the fluxes at the outlets ($\mathbf{n} \cdot \mathbf{u}_p > 0$). On a solid wall, all convective fluxes vanish due to the strongly enforced no-penetration condition $\mathbf{n} \cdot \mathbf{u}_p = 0$.

3.3. Source Term Update

The first step of the Douglas-Rachford scheme (25)–(26) is followed by an implicit correction of the involved interphase transfer terms. In this step, the drag force and heat exchange term are discretized in semi-implicit fashion. First, the velocities are updated by solving the linear system

$$(\alpha_p\rho_p)^* \frac{\mathbf{u}_p^{n+1} - \mathbf{u}_p^*}{\Delta t} = \gamma_D^*(\mathbf{u}_g^{n+1} - \mathbf{u}_p^{n+1}) - \mathbf{f}_D^n, \tag{33}$$

$$(\alpha_g\rho_g)^* \frac{\mathbf{u}_g^{n+1} - \mathbf{u}_g^*}{\Delta t} = \gamma_D^*(\mathbf{u}_p^{n+1} - \mathbf{u}_g^{n+1}) + \mathbf{f}_D^n, \tag{34}$$

where the superscript $*$ refers to the solution of system (25) and

$$\gamma_D^* = \frac{3}{4} C_D^* \frac{\rho_g^*}{d} \alpha_p^* |\mathbf{u}_g^* - \mathbf{u}_p^*|. \tag{35}$$

Once the velocities have been updated, the changes in energy due to the interphase drag and heat exchange are taken into account as follows:

$$(\alpha_p\rho_p)^* \frac{E_p^{n+1} - E_p^*}{\Delta t} = \gamma_T^*(T_g^{n+1} - T_p^{n+1}) - \tilde{q}_T^n, \tag{36}$$

$$(\alpha_g\rho_g)^* \frac{E_g^{n+1} - E_g^*}{\Delta t} = \gamma_T^*(T_p^{n+1} - T_g^{n+1}) + \tilde{q}_T^n. \tag{37}$$

The heat transfer coefficient γ_T^* and net source/sink $\tilde{q}_T^n$ are given by

$$\gamma_T^* = \frac{Nu^* 6\kappa_g}{d^2} \alpha_p^*, \qquad \tilde{q}_T^n = q_T^n + \mathbf{u}_p^{n+1} \cdot \mathbf{f}_D^{n+1} - \mathbf{u}_p^n \cdot \mathbf{f}_D^n. \tag{38}$$

Since mass transfer is neglected, there are no source terms in the continuity equations. Therefore, the effective densities $(\alpha\rho)_k^{n+1} := (\alpha\rho)_k^*$ remain unchanged.

4. Numerical Results

A preliminary verification of the above fractional-step algorithm was performed in two dimensions. Simulation results for a time-dependent compression corner problem and for a stationary particle-laden nozzle flow are presented in this section. A good qualitative agreement with numerical studies published in the literature [1, 8, 13, 14] is observed.

4.1. Compression Corner

The first test problem to be used for preliminary verification purposes is an unsteady two-phase counterpart of the compression corner benchmark. The proposed algorithm is readily applicable, although it was designed primarily for steady-state computations. To achieve higher accuracy for nonstationary problems, second-order time integration / operator-splitting schemes and limiters based on the flux-corrected transport (FCT) algorithm should be employed.

The computational domain consists of a rectangular driver section and a trapezoidal driven section in which the slope of the lower wall corresponds to the angle $\theta = 27^\circ$. The relevant parameter values and initial data are listed in Tables 1–3. In the driver section, a homogeneous mixture of air with a very small amount of particles is flowing parallel to the walls of the channel. Here, the solution is initialized by the freestream conditions and remains unchanged during the entire simulation. In the driven section, the initial velocity is zero, the density and temperature of gas are lower, and the mass fraction of particles is as high as 0.5. Initially, the gas and particles are in thermal equilibrium ($T_p = T_g$). The solution of the so-defined Riemann problem is a $M_s = 2.03$ shock.

μ	$1.65 \cdot 10^{-5}\, Pa\, s$
c_{vp}	$1380\, \frac{J}{kg\, K}$
c_{vg}	$718\, \frac{J}{kg\, K}$
c_{pg}	$1010\, \frac{J}{kg\, K}$
Pr	0.75
d	$2 \cdot 10^{-6}\, m$
γ	1.4
ρ_p	$4000\, \frac{kg}{m^3}$

Table 1: Input constants.

ρ_g	$0.39\, \frac{kg}{m^3}$
$\lvert \mathbf{u}_g \rvert$	$334.12\, \frac{m}{s}$
T_g	$299.2\, K$

Table 2: Initial data (driver section).

ρ_g	$0.15\, \frac{kg}{m^3}$
$\lvert \mathbf{u}_g \rvert$	$0.0\, \frac{m}{s}$
T_g	$177.55\, K$

Table 3: Initial data (driven section).

The simulation is performed with $163,840$ bilinear elements using the time step $\Delta t = 10^{-7}\, s$ until the final time $T = 8 \cdot 10^{-4}\, s$. The diagram in Fig.1a is a snapshot of the effective gas density. For comparison purposes, the density distribution for the pure gas flow at the same conditions is presented in Fig.1b. It can be seen that the work of the drag force and heat

exchange result in a significant reduction of the shock speed in the case of the particle-laden flow. This phenomenon was also observed in [8, 14]. The effective density and temperature of particles are depicted in Fig.1c and Fig.1d, respectively.

4.2. JPL Nozzle Flow

The second example is concerned with a steady particle-laden gas flow in a Jet Propulsion Laboratory (JPL) nozzle. The geometry of the domain is described, e.g., in [13]. The left part is a chamber with a homogeneous mixture of gas and particles at equilibrium conditions. The gas in the chamber is at high pressure, and the flow accelerates in the middle of the nozzle. Due to the drag force, the particles exhibit the same qualitative behavior.

Although the solution is smooth, the presence of curved boundaries and a subsonic inlet require a careful implementation of boundary conditions. Moreover, the coexistence of low Mach number zones with local supersonic regions implies that the numerical algorithm must be able to handle both strongly and weakly compressible flows efficiently. The wide range of Mach numbers causes a high stiffness, which calls for the use of implicit schemes and makes the problem at hand very challenging.

In our numerical experiment, we use the parameter values listed in Table 1. An additional computation with $d = 20 \cdot 10^{-6} m$ is performed for comparison purposes. At the inlet, the volume fraction of particles equals $\alpha_p = 10^{-4}$, and first three Riemann invariants for the gas phase are

$$W_1 = -2546.1554, \quad W_2 = 79533.0583, \quad W_3 = 0.0. \tag{39}$$

Since the fourth wave is leaving the domain, W_4 is computed numerically.

Steady-state solutions are computed using 283, 648 linear elements. The results in Fig. 2a and Fig. 2b depict the effective particle density for $d = 2 \cdot 10^{-6} m$ and $d = 20 \cdot 10^{-6} m$, respectively. In the diverging part of the JPL nozzle, particle-free boundary layers arise in the vicinity of the walls. The thickness of these layers increases with the particle diameter and, hence, with the decreasing magnitude of the drag force. The same behavior was observed in [1] and [13]. The stationary gas density and Mach number distribution are presented in Fig. 2c and Fig. 2d, respectively.

5. Conclusions and Outlook

The two-fluid model of compressible particle-laden gas flows was discretized using an implicit high-resolution finite element scheme. A mul-

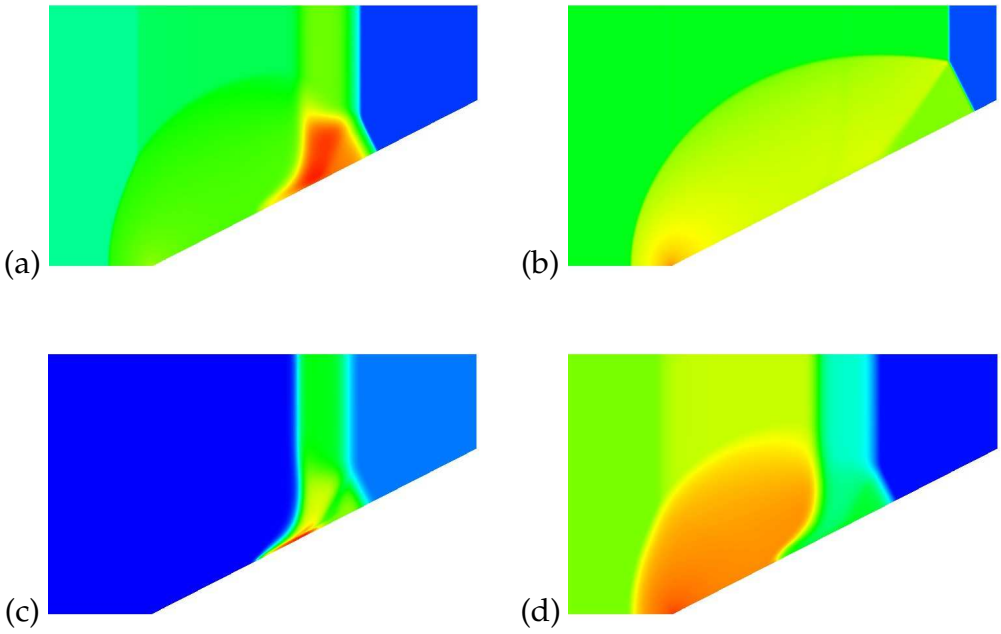

Figure 1: Compression corner, solutions at $T = 8 \cdot 10^{-4}\, s$.

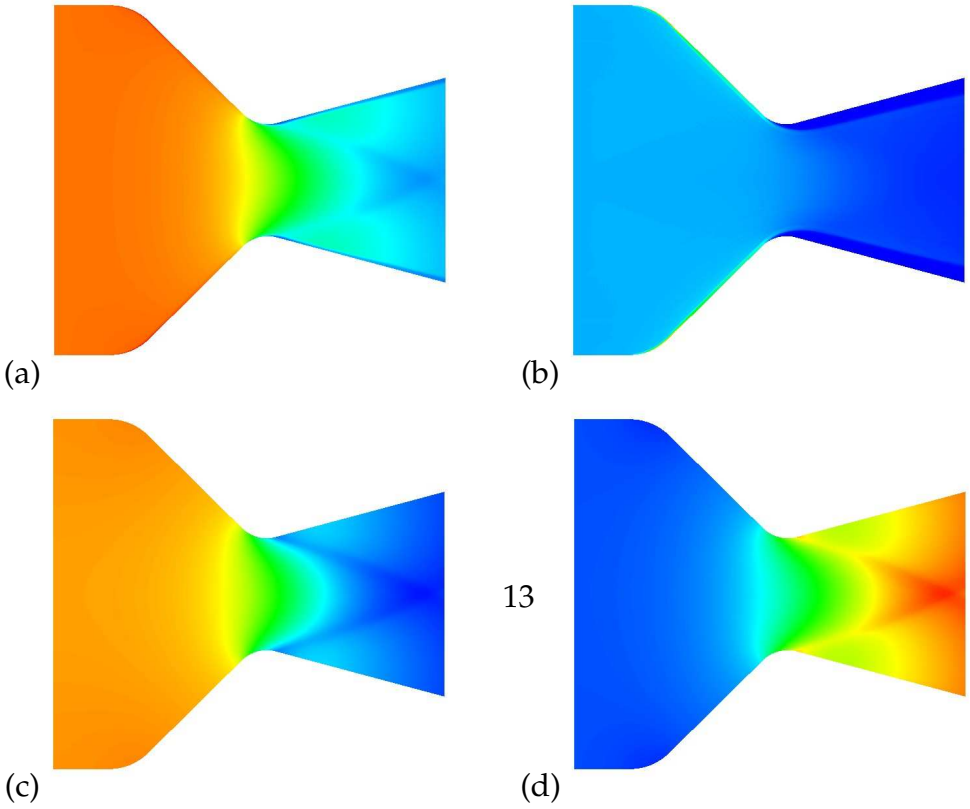

Figure 2: JPL nozzle, steady-state solutions.

tidimensional flux limiter of TVD type was implemented to enforce positivity constraints at the discrete level. The interphase transfer terms were included making use of the Douglas-Rachford splitting. A fully implicit treatment of weak boundary conditions was adopted to maintain robustness and secure convergence of nonlinear iterations. The performance of the proposed fractional-step algorithm was illustrated by numerical results.

Further research will focus on the implementation of a linearized semi-implicit Newton-like time-stepping scheme [3, 2, 6] as an efficient alternative to solving nonlinear algebraic systems at each (pseudo-)time step. The Douglas-Rachford splitting is unconditionally stable but the time steps must be relatively small to achieve convergence in steady state computations. Therefore, the use of operator splitting will be restricted to time-dependent flow problems in the future. The strongly coupled semi-implicit algorithm to be presented in a forthcoming paper is to be recommended for stationary problems because it is stable and convergent for arbitrarily large CFL numbers. A further acceleration of convergence rates can be obtained with nonlinear multigrid techniques. Unsteady flows will be simulated using time-stepping / operator-splitting schemes of second order and algebraic flux correction of FCT type. The developed methods and software provide a useful tool for investigation of thermal spraying processes and other two-phase flow problems.

References

[1] I. Chang: One- and two-phase nozzle flows, AIAA J., Vol. 18, Issue 12, 1980, Article No. 80-0272R.

[2] V. Dolejsi, M. Feistauer: A semi-implicit discontinuous Galerkin finite element method for the numerical solution of inviscid compressible flow, J. Comput. Phys., Vol. 198, 2004, pp. 727–746.

[3] A. Nejat: A higher-order accurate unstructured finite volume Newton-Krylov algorithm for inviscid compressible flows, PhD thesis, 2007

[4] J. Douglas, H. H. Rachford: On the numerical solution of heat con-

duction problems in two or three space variables, Trans. Amer. Math. Soc., Vol. 82, 1956, pp. 421–439.

[5] D. Drew, S. L. Passmann: Theory of Multicomponent Fluids, Springer, 1999.

[6] M. Feistauer, V. Kučera: On a robust discontinuous Galerkin technique for the solution of compressible flow, J. Comput. Phys., Vol. 224, 2007, pp. 208–221.

[7] C. Hirsch: Numerical Computation of Internal and External Flows, Computational Methods for Inviscid and Viscous Flows, Vol. 2, Wiley, 1990.

[8] S. W. Kim, K. S. Chang: Reflection of shock wave from a compression corner in a particle-laden gas region, Shock Waves, Issue 1, 1991, pp. 65-73.

[9] L. Krivodonova, M. Berger: High-order accurate implementation of solid wall boundary conditions in curved geometries. J. Comput. Phys. Vol. 211, 2006, pp. 492–512.

[10] D. Kuzmin, R. Löhner and S. Turek (eds.) Flux-Corrected Transport: Principles, Algorithms, and Applications. Springer, 2005, pp. 155–250.

[11] D. Kuzmin, Algebraic flux correction for finite element discretizations of coupled systems. In: E. Oñate, M. Papadrakakis and B. Schrefler (eds.) Computational Methods for Coupled Problems in Science and Engineering II, CIMNE, Barcelona, 2007, pp. 653–656.

[12] E. Loth, S. Sivier, J. Baum: Dusty Detonation Simulations with Adaptive Unstructured Finite Elements AIAA Journal, Vol. 35, 1997, pp. 1018–1024.

[13] M. Nishida, S. Ishimaru: Numerical analysis of gas-solid two-phase nonequilibrium nozzle flows, JSME Int. J., Series 2, Vol. 33, Issue 3, 1990, pp. 494–500.

[14] J. S. Park, S. W. Baek: Interaction of a moving shock wave with a two-phase reacting medium, Int. J. Heat Mass Trans., Vol. 46, 2003, pp. 4717–4732.

[15] M. Pelanti, R. J. Leveque: High-Resolution finite volume methods for dusty gas jets and plumes, SIAM J. Sci. Comput., Vol. 28, Issue 4, 2006, pp. 1335–1360.

[16] L. Sainsaulieu: Finite volume approximations of two-phase fluid flows based on an approximate Roe-type Riemann solver, J. Comput. Phys., Vol. 121, 1995, pp. 1–28.

[17] R. Saurel, R. Abgrall: A multiphase Godunov method for compressible multifluid and multiphase flows, J. Comput. Phys., Vol. 150, 1999, pp. 425–467.

[18] S. Sivier, E. Loth, J. Baum, R. Löhner: Unstructured adaptive remeshing finite element method for dusty shock flow, Shock Waves, Issue 4, 1999, pp. 15–23.

[19] V. Selmin, L. Formaggia: Unified construction of finite element and finite volume discretizations for compressible flows, Int. J. Num. Meth. Eng., Vol. 39, 1996, pp. 1–32.

[20] J.-Y. Trepanier, M. Reggio, D. Ait-Ali-Yahia: An implicit flux-difference splitting method for solving the Euler equations on adaptive traingular grids, Int. J. Num. Meth. Heat Fluid Flow, Vol. 3, 1993, pp. 63–77.